



Cite this: *Chem. Commun.*, 2016, 52, 8730

Received 1st May 2016,
Accepted 8th June 2016

DOI: 10.1039/c6cc03629e

www.rsc.org/chemcomm

Novel layered $\text{Li}_3\text{V}_2(\text{PO}_4)_3/\text{rGO}\&\text{C}$ sheets as high-rate and long-life lithium ion battery cathodes†

Qiulong Wei,‡ Yanan Xu,‡ Qidong Li, Shuangshuang Tan, Wenhao Ren, Qinyou An* and Liqiang Mai*

Novel layered $\text{Li}_3\text{V}_2(\text{PO}_4)_3/\text{rGO}\&\text{C}$ sheets are synthesized by novel interfacial modified assembly, freeze-drying and confined annealing processes. The uniform LVP layers are alternated with rGO&C layers to form the composite layered structure, providing effective electron and ion transport. As a lithium-ion battery cathode, the composite displays excellent electrochemical performance.

To meet the high requirement of lithium-ion batteries (LIBs) for hybrid electric vehicles (HEVs), electric vehicles (EVs), and large-scale energy storage systems (EESs), the electrochemical performance (especially rate capabilities) of both cathodes and anodes needs to be further improved.¹ Lithium transition-metal phosphates have attracted tremendous attention as high performance cathodes for rechargeable LIBs, owing to their high theoretical specific capacity, high operating voltage, good structural stability and abundance in nature.² Among them, monoclinic $\text{Li}_3\text{V}_2(\text{PO}_4)_3$ (LVP) possesses three-dimensional (3D) fast Li^+ ion insertion/extraction tunnels, leading to a very high ion diffusion coefficient (10^{-9} – 10^{-10} $\text{cm}^2 \text{s}^{-1}$), much higher than that of LiFePO_4 (10^{-14} – 10^{-16} $\text{cm}^2 \text{s}^{-1}$).^{3,4} The fast ion diffusion kinetics is beneficial to its rate performance. However, the separated $[\text{VO}_6]$ octahedral arrangements result in the poor electronic conductivity of LVP (2.4×10^{-7} S cm^{-1}), which indeed hinders its rate capabilities.^{3,4}

Carbon coating and the recent reduced graphene oxide (rGO) modification exhibit the improvement of the electrochemical performance for LVP in LIBs;⁵ however, their performance still needs to be further improved. The irregular carbon coating or general rGO nanosheet (rGO-NSSs) mixed composite leads to unsatisfactory connectivity with active materials and hence low capacity.^{4a,5b} Rational design and synthesis of novel LVP with carbon or/and rGO composite structures is proposed to be an effective strategy to

achieve high performance.^{4,6} Employing conductive rGO-NSSs as matrices to form conductive networks is beneficial to electron transport.^{6a} Furthermore, an ideal structure model, that is active material/rGO composite layered structure, is demonstrated as the high performance electrode structure.^{6a,7} However, this composite layered structure has not been reported for the LVP cathode.

Herein, we present a novel and facile interfacial modified synthesis method for preparing layered LVP/rGO&C sheets, in which the LVP layers are uniformly alternated with rGO&C layers. The rGO&C layers offer facile and rapid electron transport while the open crystal structure of LVP provides 3D ion diffusion pathways, realizing matched electron and ion transfer processes and then remarkable rate capabilities. Meanwhile, the as-synthesized LVP/rGO&C sheets are highly stable, leading to excellent cycling performance.

Fig. 1 schematically illustrates the synthesis process of the layered LVP/rGO&C sheets (the detailed synthesis process is in the ESI†). In brief, the $\text{V}(\text{acac})_3$, Li_2CO_3 and $\text{NH}_4\text{H}_2\text{PO}_4$ are dissolved in deionized water followed by a hydrothermal treatment. After that, LVP jelly-like gels are obtained (Fig. S1, ESI†). The zeta potential of LVP gels is -42.1 mV, indicating stable dispersions of colloids with negative charge. The graphene oxide nanosheets (GO-NSSs) are prepared by the modified Hummers method (ESI†).^{6d} The GO-NSSs with abundant functional groups and negative charge on their surface exhibit a zeta potential of -36.6 mV in aqueous solution.^{6b} After rapidly mixing them, owing to the hydrogen bonding, and amphiphilic and coulombic interactions between LVP colloids and GO-NSSs,^{6b} the LVP colloids are uniformly surround the well dispersed GO-NSSs. The mixture displays a zeta potential of -40.6 mV.

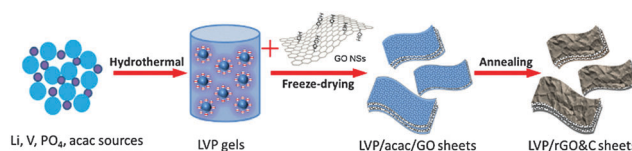


Fig. 1 Schematic synthesis procedure of layered LVP/rGO&C sheets.

State Key Laboratory of Advanced Technology for Materials Synthesis and Processing, Wuhan University of Technology, Wuhan 430070, China.

E-mail: mlq518@whut.edu.cn, anqinyou86@whut.edu.cn

† Electronic supplementary information (ESI) available: Experimental details and supplementary figures. See DOI: 10.1039/c6cc03629e

‡ Q. L. Wei and Y. N. Xu contributed equally to this work.

After freeze-drying, the well mixed LVP gels/GO structures are duplicated, while the sheet morphology (Fig. S2, ESI†) is owing to the ice template effect during the freeze-drying process.⁸ During annealing in a reducing atmosphere, the pyrolysis of added organics (acac) turns into amorphous carbon and GO-NSs are reduced to rGO-NSs. At this point, the formation and growth of LVP crystals are confined by the rGO&C matrices, resulting in layered LVP/rGO&C sheets. The LVP/C sheets without rGO-NSs are also prepared for comparison (ESI†).

X-ray diffraction (XRD) patterns of LVP/rGO&C and LVP/C sheets are displayed in Fig. S3a, ESI†. The diffraction peaks of both samples are well indexed to the monoclinic LVP phase (JCPDS No. 01-072-7074) with a space group of $P2_1/n$. Raman spectra were recorded to further study the nature of carbon formed in the samples (Fig. S3b, ESI†).⁴ Two peaks located at around 1330 and 1580 cm^{-1} are attributed to the D-band (disordered carbon) and the G-band (graphitic carbon), respectively. The intensity ratio of I_D/I_G for LVP/C and LVP/rGO&C is 1.06 and 1.30, respectively, indicating an increased graphitic degree in LVP/rGO&C owing to the presence of rGO-NSs.⁴ The carbon content of LVP/C and LVP/rGO&C is only 1.4% and 4.5%, respectively, determined by CHN analysis. The Brunauer–Emmett–Teller (BET) specific surface area (SSA) of LVP/rGO&C and LVP/C is 6.9 and 4.2 $\text{cm}^2 \text{g}^{-1}$, respectively. The slightly higher SSA of LVP/rGO&C is due to the higher carbon content.

Scanning electron microscopy (SEM) and transmission electron microscopy (TEM) were used to characterize the morphology and detailed structure of samples. The LVP/rGO&C composites (Fig. 2a) retain their sheet morphology after annealing (Fig. S2, ESI†). From the scanning TEM-high-angle annular dark-field (STEM-HAADF) image (Fig. 2b), it is found that the sheets are composed of interconnected LVP particles enriched with pores. The STEM-energy dispersive spectroscopy (STEM-EDS) mappings (Fig. 2c) confirm the uniform distribution of V, O, P and C. The TEM images (Fig. 2d and e) show the LVP particles in between the C/rGO matrices. The high resolution TEM (HRTEM) image (Fig. 2e, inset) shows the interplanar spacing of the crystals of 0.294 nm, corresponding to the (221) plane of LVP crystals, and the amorphous carbon layers. The LVP/C sheets exhibit similar morphology with the LVP/rGO&C (Fig. S4, ESI†). The carbon structure formed in layered LVP/rGO&C sheets is further investigated by removing the LVP and retaining the rGO&C matrices.⁴ The rGO&C matrices still display sheet morphology after removing the LVP layers (Fig. 2f). In a high magnification SEM image (Fig. 2g), the rGO-NSs are uniformly distributed on the rGO&C layers. However, for the carbon that remained in the LVP/C sample (Fig. S5, ESI†), the carbon matrices are smooth. From the cross section (Fig. 2h), a layered rGO&C structure is clearly observed, while the empty spaces originate from the removal of LVP particles. The above results demonstrate that the LVP particles alternated with rGO&C matrices with strong contact, forming layered LVP/rGO&C sheets (Fig. 2i).

The electrochemical performance of the LVP/rGO&C sheets and LVP/C sheets was measured in CR2016 coin cells. The first charge/discharge curves of LVP/rGO&C and LVP/C at a rate of 1C ($1\text{C} = 133 \text{ mA h g}^{-1}$) in 3–4.3 V are shown in Fig. 3a.

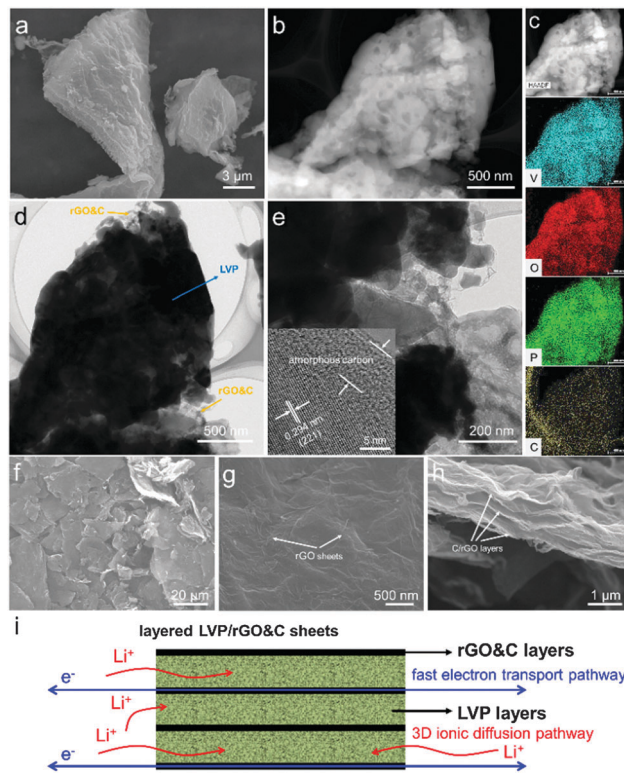


Fig. 2 SEM (a), STEM-HAADF (b), STEM-EDS mappings (c) TEM (d and e), and HRTEM (inset of e) images of layered LVP/rGO&C sheets. (f–h) SEM images of the remained rGO&C matrices after removing the LVP layers. (i) Schematic of the layered LVP/rGO&C sheets.

Both samples exhibit three pairs of plateaus, corresponding to the reversible phase transitions of $\text{Li}_3\text{V}_2(\text{PO}_4)_3 \leftrightarrow \text{Li}_{2.5}\text{V}_2(\text{PO}_4)_3 \leftrightarrow \text{Li}_2\text{V}_2(\text{PO}_4)_3 \leftrightarrow \text{Li}_1\text{V}_2(\text{PO}_4)_3$.⁴ The LVP/rGO&C cathode displays longer charge/discharge plateaus and lower overpotentials than those of LVP/C, indicating a deeper and more reversible reaction in LVP/rGO&C. The initial discharge capacity of LVP/rGO&C is 131 mA h g^{-1} (extremely close to the theoretical capacity of 133 mA h g^{-1} with two lithium ions inserted/extracted per mole), higher than the capacity of 106 mA h g^{-1} for LVP/C. The initial coulombic efficiency of LVP/rGO&C is $\sim 98.8\%$, indicating highly reversible Li^+ insertion/extraction processes. After 100 cycles, the capacity retention of LVP/rGO&C sheets is 95.4%, which is higher than that of LVP/C sheets (93.4%), indicating the better cycling stability of LVP/rGO&C (Fig. 3b). Even after 1000 cycles at 1C, the capacity retention of LVP/rGO&C is still 87.0%, displaying excellent cycling performance.

The rate performance was further investigated (Fig. 3c). The LVP/rGO&C sheets exhibit better rate capability than that of LVP/C sheets and commercialized LiFePO_4/C powders (Fig. S7, ESI†). At a high rate of 20C, a discharge capacity of 109 mA h g^{-1} is obtained, almost 1.63 times of the LVP/C (67 mA h g^{-1}). Even at higher rates of 50, 80 and 100C, the LVP/rGO&C also delivers a high capacity of 102, 78 and 63 mA h g^{-1} , respectively, showing excellent high rate capability. After the increased current rates, 97.7% of the initial capacity for LVP/rGO&C is recovered when the rate changes back to 0.5C.

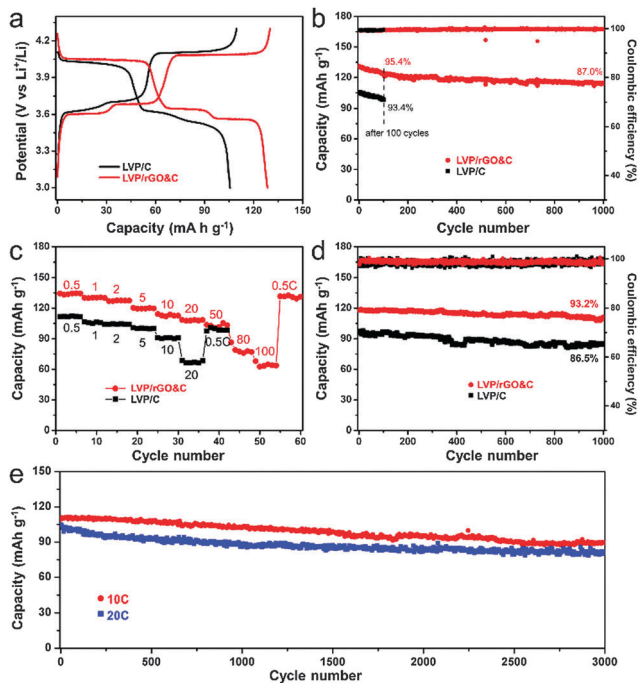


Fig. 3 The initial charge–discharge curves at 1C (a), cycling performance at 1C (b), rate performance (c) and cycling performance at 5C (d) of LVP/rGO&C and LVP/C, respectively. (e) Cycling performance of LVP/rGO&C at 10C and 20C.

Electrochemical impedance spectroscopy (EIS) was measured to investigate the electrochemical reaction kinetics of the two samples.^{4,9} The Nyquist plots (Fig. S6, ESI†) show a depressed semicircle (which represents charge transfer resistances R_{ct}) and a slanted line (which represents the Warburg impedance that refers to ion diffusion ability).⁶ The LVP/rGO&C exhibits a much lower R_{ct} value than that of LVP/C, indicating a better charge transfer ability of LVP/rGO&C composites. The increased reaction kinetics is owing to the much higher electron conductivity of rGO&C matrices and strong contact between LVP and matrices, which provides effective electron transport. Meanwhile, the high ion conductive nature of the LVP crystal structure and the pores in the composites ensure rapid ion diffusion. The combination of the above two advantages results in the remarkable rate performance of layered LVP/rGO&C sheets (Fig. 2i), whose rate capacities are better than most of the state-of-the-art reported results.^{4a,5a,c,10}

Long-term cycling performance at a rate of 5C is subsequently measured (Fig. 3d). The LVP/rGO&C displays an initial discharge capacity of 118 mA h g^{-1} , and a capacity retention of 93.2% after 1000 cycles is obtained. Both the capacity and the capacity retention of LVP/rGO&C are much higher than those of the LVP/C. Furthermore, at higher rates of 10C and 20C, the LVP/rGO&C still displays excellent cycling performance with capacity retention of 81.8% and 77.1% after 3000 cycles, respectively (Fig. 3e). The remarkably high rate cycling performance is ascribed to the unique structure, in which interconnected LVP

particles are well embedded in the layered rGO&C matrices to form a stable structure for accommodating the volume changes. In addition, the rGO&C matrices are able to prevent the dissolution of vanadium during cycling, thus extending the cycle life.^{6a,11}

In summary, we present a facile method to fabricate the novel layered LVP/rGO&C sheets, in which LVP layers (interconnected LVP particles) are alternated with rGO&C layers. The LVP/rGO&C sheets present remarkably high rate performance with a high capacity of 102 and 63 mA h g^{-1} even at 50C and 100C, respectively, overcoming the main issue of rate capability for the LVP cathode. Meanwhile, the layered composites display excellent long-term cycling life (81.8% retention after 3000 cycles at a rate of 10C). Our work demonstrates that the layered LVP/rGO&C sheets are very promising cathodes for high-performance LIBs. This kind of effective design and synthesis strategy can also be extended to other promising cathode or anode materials for advanced energy storage applications.

We gratefully acknowledge the National Basic Research Program of China (2013CB934103), National Science Fund for Distinguished Young Scholars (51425204), National Natural Science Foundation of China (51521001), Hubei Province Natural Science Fund for Distinguished Young Scholars (2014CFA035), and the International Postdoctoral Exchange Fellowship Program (201600250).

Notes and references

- 1 L. Mai, X. Tian, X. Xu, L. Chang and L. Xu, *Chem. Rev.*, 2014, **114**, 11828–11862.
- 2 (a) M. S. Whittingham, *Chem. Rev.*, 2014, **114**, 11414–11443; (b) Z. Jian, W. Han, Y. Liang, Y. Lan, Z. Fang, Y.-S. Hu and Y. Yao, *J. Mater. Chem. A*, 2014, **2**, 20231–20236; (c) J. Wang, Z. Wang, X. Li, H. Guo, X. Wu, X. Zhang and W. Xiao, *Electrochim. Acta*, 2013, **87**, 224–229.
- 3 (a) C. Liu, R. Massé, X. Nan and G. Cao, *Energy Storage Mater.*, 2016, **4**, 15–58; (b) L. Chen, B. Yan, J. Xu, C. Wang, Y. Chao, X. Jiang and G. Yang, *ACS Appl. Mater. Interfaces*, 2015, **7**, 13934–13943.
- 4 (a) Q. Wei, Q. An, D. Chen, L. Mai, S. Chen, Y. Zhao, K. M. Hercule, L. Xu, A. Minhas-Khan and Q. Zhang, *Nano Lett.*, 2014, **14**, 1042–1048; (b) Y. Luo, X. Xu, Y. Zhang, Y. Pi, Y. Zhao, X. Tian, Q. An, Q. Wei and L. Mai, *Adv. Energy Mater.*, 2014, **4**, 1400107.
- 5 (a) H. Liu, P. Gao, J. Fang and G. Yang, *Chem. Commun.*, 2011, **47**, 9110–9112; (b) B. Pei, Z. Jiang, W. Zhang, Z. Yang and A. Manthiram, *J. Power Sources*, 2013, **239**, 475–482; (c) H. Liu, G. Yang, X. Zhang, P. Gao, L. Wang, J. Fang, J. Pinto and X. Jiang, *J. Mater. Chem.*, 2012, **22**, 11039; (d) X. Rui, D. Sim, K. Wong, J. Zhu, W. Liu, C. Xu, H. Tan, N. Xiao, H. H. Hng, T. M. Lim and Q. Yan, *J. Power Sources*, 2012, **214**, 171–177.
- 6 (a) R. Raccichini, A. Varzi, S. Passerini and B. Scrosati, *Nat. Mater.*, 2015, **14**, 271–279; (b) D. Wu, F. Zhang, H. Liang and X. Feng, *Chem. Soc. Rev.*, 2012, **41**, 6160–6177; (c) Y. Zhou, X. Rui, W. Sun, Z. Xu, Y. Zhou, W. J. Ng, Q. Yan and E. Fong, *ACS Nano*, 2015, **9**, 4628–4635; (d) Y. Zhao, J. Feng, X. Liu, F. Wang, L. Wang, C. Shi, L. Huang, X. Feng, X. Chen, L. Xu, M. Yan, Q. Zhang, X. Bai, H. Wu and L. Mai, *Nat. Commun.*, 2014, **5**, 4565.
- 7 W. Li, F. Wang, Y. Liu, J. Wang, J. Yang, L. Zhang, A. A. Elzatahry, D. Al-Dahyan, Y. Xia and D. Zhao, *Nano Lett.*, 2015, **15**, 2186–2193.
- 8 Q. Wei, J. Liu, W. Feng, J. Sheng, X. Tian, L. He, Q. An and L. Mai, *J. Mater. Chem. A*, 2015, **3**, 8070–8075.
- 9 Z. Jian, M. Zheng, Y. Liang, X. Zhang, S. Gheyhani, Y. Lan, Y. Shi and Y. Yao, *Chem. Commun.*, 2015, **51**, 229–231.
- 10 L. Wang, J. Bai, P. Gao, X. Wang, J. P. Looney and F. Wang, *Chem. Mater.*, 2015, **27**, 5712–5718.
- 11 Y. Wang, J. Zeng, X. Cui, L. Zhang and G. Zheng, *Small*, 2016, **12**, 1091–1097.